Supplementary Materials for

Sulfate Burial Constraints on the Phanerozoic Sulfur Cycle

Itay Halevy,* Shanan E. Peters, Woodward W. Fischer

*To whom correspondence should be addressed. E-mail: itay.halevy@weizmann.ac.il

This PDF file includes:

Materials and Methods
Supplementary Text
Figs. S1 to S5
Caption for Database S1
References (*35–46*)

Other Supplementary Material for this manuscript includes the following:
(available at www.sciencemag.org/cgi/content/full/337/6092/331/DC1)

Database S1 as comma-separated, plain text file:
Data and model fluxes binned in 5-Myr intervals

Materials and Methods

Macrostratigraphic Estimates of Sulfate Evaporite Burial Rates

The Macrostrat database (http://macrostrat.org) is built primarily on published stratigraphic correlation charts for the U.S.A., Canada, and the Caribbean region and resolves the surface and subsurface stratigraphic record spatially and temporally into hiatus-bound rock packages of known lithology (19, 35-37). Among other properties, the database estimates the area and thickness of rock units, provides age estimates for their upper and lower boundaries and contains information about dominant and subordinate lithologies. Using deposit area and thickness estimates, we calculated deposit volumes. We assumed that each subordinate lithology (up to four) accounts for 10% of the volume and that the remainder is divided among the dominant lithologies. The volume fractions were translated into abundance (in moles) using the molecular weight and density of gypsum ($CaSO_4 \times 2H_2O$, ρ=2.32 g cm^{-3}, M_w=172 g mole^{-1}) and anhydrite ($CaSO_4$, ρ=2.97 g cm^{-3}, M_w=136 g mole^{-1}), depending on which of these minerals is indicated in the lithologic database fields. In a minority of database entries the lithology is listed as "evaporites" instead of a specific sulfate mineral. As the majority of sulfate evaporites in the database are composed of anhydrite, in such cases we assigned anhydrite as the dominant sulfate mineralogy. The data, binned in 5 Myr intervals, are given in table S1.

We binned the data by age. Using age estimates for the deposits' upper and lower boundaries we divided deposits that were split between two or more intervals in proportion to the fraction of time residing in each of the bins, conserving sulfate evaporite mass. For example, a deposit with a lower boundary age of 8 Ma and an upper boundary age of 4 Ma would be apportioned 25% into the 0–5 Ma bin and 75% into the 5–10 Ma bin. We then divided the amount of sulfate deposited in each of the bins by the bin duration to obtain deposition rate estimates. Larger bin durations decrease variability in the deposition rates by averaging high and low values, but there is no relationship apparent between average deposition rates and bin size (Fig S2).

Correction for Weathering

It has been hypothesized that the mass of sedimentary rocks preserved in the record decays exponentially since the time of their deposition (38). Weathering rates vary with sedimentary rock type, with evaporites being especially susceptible to dissolution by marine and meteoric waters. We account for this effect by multiplying the estimated sulfate evaporite abundances by an age-dependent factor, e^{kt}, where t is the age of the deposits and k is the first order decay rate constant. The value of k for clastic rocks has been estimated to be ~0.001 Myr^{-1} (39), whereas the value estimated for halite, which is much more easily dissolved and weathered, is ~0.003 (40). Because of uncertainties in the exact values for the decay constants suggested for marine rocks, we bracket values of k between 0.000 (i.e., no decay) and 0.003, with a default value of 0.002 that accounts for the greater solubility of sulfate evaporites relative to siliciclastic and carbonate rocks, and the lesser solubility relative to halite. The sensitivity to this choice is included in the uncertainty envelopes in Figs. 1 and 2 of the main text.

Scaling from North America and the Caribbean to the Globe

The richness of the macrostratigraphic database affords an unprecedented estimate of variability in sediment volume in North America and the Caribbean (NAC; Fig. S3). However, to obtain global rates of sulfate evaporite burial, the data must be scaled from NAC to the globe. We did this by establishing mechanistic relationships between the NAC observations and *i*) the area of submerged continental crust at latitudes of net evaporation and *ii*) eustatic sea level change. We used these relationships together with the global area of submerged continental crust and the sea level curve to estimate global sulfate burial rates. Below we describe the approach and discuss its uncertainties.

The formation of sulfate evaporite deposits requires hydrographic isolation and evaporation of marine-fed sedimentary basins (22). For the deposits to be stratigraphically significant, episodic recharge of seawater (or another salt-containing solution) is necessary. These conditions are met at latitudes of net evaporation (22), in several basin settings:

1. Rift zones: During the early stages of continental breakup, seawater floods the actively thinning and subsiding continental crust, forming shallow seaways that can become partially isolated from the ocean (e.g., Jurassic-Cretaceous Gulf of Mexico, Miocene Red Sea).
2. Prograding shorelines: Inflow and deposition of sediments as rivers enter the ocean generate large, poorly drained floodplains as well as shallow basins where local barriers to circulation may form. This often occurs especially at times of tectonic stability, during the middle to late lifetime of slowly subsiding continental shelves (e.g., Holocene evaporites in the Arabian Gulf).
3. Continental collision zones: As continents collide, differential uplift and subsidence may isolate large basins, restricting mixing with the ocean (e.g., Neogene evaporites in the Mediterranean Sea and the Carpathian Foredeep Basin, and the Permian basins of west Texas).

In addition to these settings, intracratonic basins where salt-bearing solutions are supplied by overland flow or upwelling groundwater also exist, but over Phanerozoic time these basins have contained evaporite volumes that were more than an order of magnitude smaller than the marine-fed basins (22).

Evaporite basins in the geologic record differ in their regional tectonics, local climate, basin hydrology and, possibly, other factors. However, common to the majority of basins where massive evaporites have formed over time is that they were shallow marine or coastal environments at latitudes of net evaporation (22, 41). With this in mind, we tested the correlation between our record of evaporite burial rates and the estimated Phanerozoic area of submerged continental crust as a function of latitude. We estimated the NAC and global submerged continental area from paleogeographic reconstructions, which take into account paleomagnetic constraints, sea level data, rock-type and texture, and biostratigraphy, to delineate the location of the continents and the spatial extent of submerged continental crust (21). The reconstructions record four environments (continent, upland, ocean, shallow sea), and are available in portable document format (pdf). We converted them to tagged image format (tif) and developed an algorithm to automatically calculate the area covered by shallow seas (globally and in NAC) in latitude bands of 5°.

We tested the correlation of the macrostratigraphic data with the area of NAC submerged continental crust in the latitude band ±10–50° for bins corresponding to the temporal resolution of the paleogeographic reconstructions. The first-difference correlation coefficient (Spearman's ρ) has a value of –0.30 and the p-value is 0.11. The linear product moment correlation coefficient (Pearson's r) for the untreated time series is 0.47 and increases with bin duration. At low bin durations, the linear correlation coefficient was as low as ~0.2. The moderate first-difference negative correlation suggests that in addition to the general tendency for more evaporite burial at times of high submerged continental area (the strong positive correlation between sulfate burial and submerged area), sulfate deposition tends to increase when the submerged area shrinks. This pattern is expected from a number of basin-scale processes occurring during times of high submerged continental area, such as the isolation of epicontinental seas, shoreline progradation and formation of restricted basins during continental collision. Thus, long-timescale sulfate evaporite deposition rates are well explained by the area of shallow seas at latitudes of net evaporation, but that there is substantial short-timescale variability that is not well-captured by submerged continental area and paleolatitude alone.

Changes in sea level provide important short-timescale modulation on the development of shallow restricted seas. As sea level drops, shallow marine basins may become isolated but the absence of recharge with seawater can also result in limited evaporite deposition. Furthermore, sulfate evaporites exposed by the drop in sea level are easily susceptible to weathering. In contrast, rising sea level floods continental area, generating shallow seas and preserving previously deposited sediments with ongoing deposition. Additional area suitable for sulfate deposition may eventually be created due to shoreline progradation (e.g., 42). We tested the correspondence between changes in eustatic sea level (23) and the macrostratigraphy-based evaporite deposition rates and found that approximately 30% of times of high sulfate evaporite deposition correspond to maxima in rates of sea level rise and about 45% of the times of little or no sulfate deposition correspond to rapid rates of sea level fall (Fig. S4 upper panels). Spurious correlation between two rapidly varying time series is unlikely, as only about 20% of peaks in sulfate deposition correspond to minima in sea level change and only about 10% of troughs in sulfate deposition correspond to sea level change maxima (Fig. S4 lower panels).

We regressed (ordinary least squares) the sulfate burial rate data in 5 Myr bins on the NAC submerged continental area estimates and used this relationship together with the global submerged continental area estimates to express the long-timescale (10^7–10^8 years) variability in the record. We then used the relationship between changes in sea level and the sulfate burial rate data to add short-timescale (10^5–10^7 years) variability and to generate a synthetic global sulfate evaporite burial record. The functional form of the calculated global sulfate burial rate, J_{GLOB}, is:

$$J_{GLOB} = (a{\times}A_{GLOB} + b){\times}f_{dSL},$$

where a and b are the coefficients of the linear regression on submerged continental area, A_{GLOB} is the global estimate of submerged continental area and f_{dSL} is the rate of sea level change linearly transformed to a range between 0 and 4—an empirical factor that

captures the amplitude of short-timescale variability. The NAC macrostratigraphic record and a synthetic NAC record generated using these relationships are compared in Fig. S5. The overall trend in magnitude and the amplitude of short-timescale variability are relatively well matched. The timing of burial rate maxima/minima in the synthetic record does not perfectly match the timing of maxima/minima in the stratigraphic data. This is expected because of idiosynchratic differences between regional NAC and global average sea level (23).

As mentioned above, several second-order factors governing the deposition and preservation of sulfate evaporites are not treated explicitly in the global scaling methodology we employ, such as basin hydrology and local climate. Although the macrostratigraphic dataset include lacustrine and other intracratonic basins, global scaling by the area of submerged continent does not account for these basins. This may lead to a slight underestimate of global sulfate evaporite burial rates, because such basins are known to contain a small fraction of Phanerozoic evaporite deposits (22). Paleogeographic reconstructions are available only at discrete time intervals (21), geologically brief tectonic regimes may be underrepresented. Two examples are the early stages of continental breakup and the final stages of continental collision and the closing of an ocean basin, both of which are important conditions for evaporite genesis. To accurately quantify the effect of these geologic settings on global evaporite burial would require significantly more knowledge of sedimentary geology on all continents throughout Phanerozoic time. However, because of the large areal extent and tectonic diversity of NAC and because Laurentia participated in global tectonic cycles, these settings are implicitly represented by the variability in the NAC evaporite burial rate data, which include rift, collisional and continental evaporites observed in outcrop and in the subsurface. Indeed, in the NAC data we observe rifting events to be important drivers of evaporite burial fluxes (e.g., opening of parts of the Atlantic Ocean ~125, ~160 and ~240 Ma; Fig. 1C in the main text). The only way that this approach will introduce a significant bias is if sulfate deposition was substantially less (or more) variable on the other continents than it is on NAC, which global comparisons suggest is unlikely (22).

The mole-weighted average ratio of global to NAC sulfate evaporite burial rates obtained with the scaling methodology described above is 7.2. This value of the scaling factor is in good agreement with values of ~5-8, which emerge from three different approaches. First, the ratio of the area of all continents to NAC is ~6. Second, the area-weighted ratio of global to NAC submerged continental area, based on paleogeographic reconstructions is ~7. Third, the volume-weighted average ratio of global to NAC sulfate deposits in past compilations is ~5-8 (16, 17). Based on the above analysis, the synthetic record presents a reasonable hypothesis for Phanerozoic sulfate evaporite burial rates that accurately captures the long-term rate variability and amplitude, and the correct amplitude but probably not the exact timing, of short-term variability in burial rates.

Models

All isotope mass balance models are based on the following differential equations that describe the geological sulfur cycle with a combined input from weathering and outgassing and two sedimentary sinks:

$$(1) \qquad \frac{dM}{dt} = J_{in} - J_e - J_p,$$

$$(2) \qquad \frac{dM\delta}{dt} = J_{in}\delta_{in} - J_e\delta - J_p(\delta - \Delta),$$

M is the concentration of seawater sulfate and δ is its sulfur isotopic composition, known from the fluid inclusion data and the $\delta^{34}S$ compilations, respectively (7-10). J_e and J_p are the burial fluxes of sulfate evaporite and pyrite, respectively. Δ is the average difference (in permil) between the $\delta^{34}S$ of contemporaneous sulfate evaporites and sedimentary pyrite. J_{in} is the total influx of sulfur to the ocean, comprised of contributions from evaporite weathering, oxidative weathering of sedimentary and igneous sulfides, and volcanic outgassing of sulfur volatiles. The isotopic composition of this influx, δ_{in}, depends on the relative contributions of these three components.

Several minor fluxes can be left out of these equations because they make little or no net contribution to the budget. The evaporite burial term (J_e) refers to a net flux and we do not explicitly represent gross evaporite deposition and a contribution to J_{in} from redissolution of recently deposited evaporites, which have an isotopic composition close to that of seawater sulfate. Likewise, recycling of biological sulfur emissions does not affect the net budget and is not included in J_{in}. Finally, the removal of sulfate from seawater as anhydrite in seafloor hydrothermal systems is neglected, because the anhydrite redissolves as the crust ages and cools (43). This sink for seawater sulfate is, therefore, analogous to rapidly recycled terrestrial evaporites. Estimates of the total sink of seawater sulfate to oceanic crust (as anhydrite and sulfide minerals) is about a sixth of the riverine influx and so even if as much as half of this material survives, we estimate that no more than 10% of the influx of sulfate to the ocean is accounted for by an outflux to the oceanic crust.

Equations (1) and (2) can be rewritten as:

$$(1a) \qquad \frac{dM}{dt} = J_v + J_w - J_e - J_p,$$

$$(2a) \qquad \frac{dM\delta}{dt} = J_v\delta_v + J_w\delta_w - J_e\delta - J_p(\delta - \Delta),$$

where the subscripts v and w denote the influx from volcanic outgassing and weathering, respectively. As $dM\delta/dt = \delta \times dM/dt + M \times d\delta/dt$, it is possible to substitute equation (1a) into equation (2a) to give the following:

$$(3) \qquad M\frac{d\delta}{dt} + \delta(J_v + J_w - J_e - J_p) = J_v\delta_v + J_w\delta_w - J_e\delta - J_p(\delta - \Delta).$$

Rearranging equation (3) to solve for J_p yields:

$$(4) \qquad J_p = \frac{M\dfrac{d\delta}{dt} + J_v(\delta - \delta_v) + J_w(\delta - \delta_w)}{\Delta}.$$

In the parameterized input models, equation (4) is used to calculate J_p, given parameterized values of J_w and δ_w. If J_w and δ_w are unknown, but J_p is specified, in the case for the parameterized output models, it is possible to rearrange equation (3) to solve for J_w:

$$(5) \qquad J_w = \frac{M\dfrac{d\delta}{dt} + J_v(\delta - \delta_v) - J_p\Delta}{\delta_w - \delta}.$$

Substituting this value into equation (1a) and rearranging to solve for δ_w yields:

$$(6) \qquad \delta_w = \frac{J_v\delta_v - J_e\delta - J_p(\delta - \Delta) - \dfrac{dM\delta}{dt}}{J_v - J_e - J_p - \dfrac{dM}{dt}}.$$

With $dM\mathrm{d}/dt$ and dM/dt constrained by time series fluid inclusion and $\delta^{34}S$ data, and J_e from this study, we calculate δ_w and F_w using equations (6) and then (5), respectively.

In all of the models, the values of J_v and δ_v used are 3×10^{11} mol yr^{-1} and 2‰, respectively (11, 12, 24, 44). The value of Δ is taken from (8), who used records of $\delta^{34}S$ from CAS, evaporite and barite and coeval sedimentary pyrite together with constraints on the mass-law of bacterial sulfate reduction. Below is a brief description of each of the models.

Steady State, Constant J_{in} and d_{in}

At steady state, equation (1) gives $J_{in} = J_e + J_p$. Defining $f_{pyr} \equiv J_p/(J_p + J_e)$, this can be rewritten as $J_{in} = J_p/f_{pyr}$. Substituting this into equation (2) and rearranging to solve for f_{pyr} gives:

$$(7) \qquad f_{pyr} = \frac{\delta - \delta_{in}}{\Delta}.$$

Then, $J_p = J_e \times f_{pyr}/(1 - f_{pyr})$, with J_e from this study, and equations (5) and (6) are solved for the value of J_w and δ_w required to reproduce the fluid inclusion and $\delta^{34}S$ data. The value of δ_{in} used is 8‰ VCDT (34).

Dynamic Mass Balance, Constant J_{in} and d_{in}

A model of constant input magnitude and isotopic composition can also be used in combination with the fluid inclusion and $\delta^{34}S$ time series to solve equation (4) for J_p. Then, the sulfate evaporite burial flux required for mass balance, $J_e{}^*$, is calculated using equation (1a):

$$(8) \qquad J_e^* = J_v + J_w - J_p - \frac{dM}{dt}.$$

This value is compared to J_e derived from macrostratigraphic data.

Constant and Specified f_{pyr}

$J_p = J_e \times f_{pyr}/(1 - f_{pyr})$, with J_e from this study, and equations (5) and (6) are solved for the value of J_w and δ_w required to reproduce the fluid inclusion and δ^{34}S data.

Constant and Specified J_p

With J_p specified and J_e from this study, equations (5) and (6) are solved for the value of J_w and δ_w that reproduce the fluid inclusion and δ^{34}S data. The fraction of sulfur buried as pyrite is $f_{pyr} = J_p/(J_p + J_e)$.

J_p as a Function of Submerged Continental Area

Motivated by the potential dependence of pyrite burial rates on the area of submerged continental crust, we tested a model in which J_p is related to the global submerged continental area in the following way:

$$(9) \qquad J_p = J_p^0 \times \left(\frac{A(t)}{A^0}\right)^n,$$

where J_p^0 is a prescribed default value of J_p (typically a multiple of the estimated present-day volcanic outgassing flux), $A(t)$ is the global area of submerged continental crust over Phanerozoic time, A^0 is a reference submerged continental area, taken to be the Phanerozoic average area, and n is an exponent that expresses the sensitivity of pyrite burial to submerged continental area. A zero value for n means no dependence of J_p on submerged continental area and is identical to the model of constant and specified J_p. Equations (5) and (6) are solved for the value of J_w and δ_w required to reproduce the fluid inclusion and δ^{34}S data. The fraction of sulfur buried as pyrite is $f_{pyr} = J_p/(J_p + J_e)$.

Prescribed Inputs

As with the model of constant input magnitude and isotopic composition, equation (4) is used to calculate J_p. Then, the sulfate evaporite burial flux required for mass balance, J_e^*, is calculated using equation (8) and compared to J_e derived from macrostratigraphic data. The values of inputs to the ocean in these models are given in Additional Data Table S1, at the time intervals for which the models were solved.

Model Sensitivity

We tested the sensitivity of the isotope mass balance model results to the values chosen for poorly constrained parameters (Fig. S1).

Sensitivity to the Specified Value of J_p

The default value of J_p (1.5×10^{12} mol yr^{-1}) was chosen to match estimates of present-day riverine fluxes and isotopic compositions (total influx $\sim$1.5–3.0$\times 10^{12}$ mol yr^{-1}, δ^{34}S $\sim$8‰ VCDT) in the submerged continental area-dependent and constant J_p models. This value is $\sim$5 times estimates of the volcanic outgassing flux and 40–100% of estimates for the total riverine flux of sulfate to the oceans. In the model of submerged continental area-dependent J_p, this value results in a present-day δ^{34}S value of riverine sulfate of -10.8‰ VCDT. This is much lower than existing estimates of the global average δ^{34}S of riverine sulfate because it represents the net influx (i.e., without the

contribution of recently deposited sulfate evaporites). With the recycled flux included, the δ^{34}S of riverine sulfate is +9.8‰ VCDT, close to the value estimated from assumptions about the relative contribution of sulfate weathering and oxidative weathering of sulfides to the fluxes and the isotopic composition of the weathered reservoirs (+8‰ VCDT). Indeed, measurements in some major rivers where contribution from sulfate weathering is minimal yield values of δ^{34}S similar to the model results (e.g., 45). With this default value of J_p, the Phanerozoic average value of f_{pyr} is 0.82 for both models.

At half the default value of J_p, the Phanerozoic average value of f_{pyr} is 0.71 and 0.70 for the model of constant and submerged continental area-dependent J_p, respectively (Fig. S1A). However, both models require a total J_{in} close to estimates for the volcanic influx between ~100 and 250 Ma, with values less than estimates for the volcanic influx at ~200 Ma (Fig. S1B). Consequently, we find this scenario unlikely.

At twice the default values, the Phanerozoic average value of f_{pyr} is 0.90 for both models (Fig. S1A). Values of J_{in} and δ_{in} are within reasonable ranges (Fig. S1B–C), but the estimate for the modern δ^{34}S of total riverine sulfate (including recycled sulfates) is –6.6‰ VCDT for the model of constant J_p. As mentioned above, the true isotopic composition of riverine sulfate remains uncertain, but unlikely to be as low as that required in the model of constant J_p.

Sensitivity to the Values of A^0 and n

In the model of submerged continental area-dependent J_p, the results are sensitive to both the choice of reference submerged continental area (A^0 in equation (9)) and the order of the dependence on submerged area (n in equation (9)). The former is due to an overall decrease in submerged continental area over Phanerozoic time. For example, if the modern submerged area is chosen as the reference, pyrite burial rates in the Paleozoic are high and decrease to the default value of J_p at the present day (Fig. S1D–F). With a first-order dependence of J_p on submerged continental area ($n=1$ in equation (9) as the default), the value of f_{pyr} is very similar to that in a model of constant J_p, where $n=0$ (Fig. S1D). A higher sensitivity to submerged area ($n=2,3$) results in decreasing J_p through the Phanerozoic (associated with a greater dependence to the general decrease in submerged area). The average value of f_{pyr} changes little, however, from a value of 0.82 with $n=0$ and $n=1$ to values of 0.80 and 0.78 for $n=2$ and $n=3$, respectively (Fig. S1D).

Parameterized Input with 30% Modeled Values

In the main text we hypothesized that the parameterized input models may overestimate the net influxes of sulfate into the ocean because of the weathering of recently deposited sulfates, and that the values of J_e calculated from mass balance in these models are consequently high in comparison to the macrostratigraphic estimates. We mentioned that with 30% of the modeled inputs, the value of J_e required for mass balance more closely matches the macrostratigraphic estimates in magnitude, but not in shape. This is shown in Fig. S1G–H.

Seawater Sulfate Concentration and Isotopic Composition Data

Wu *et al*., (2010) (8) recently compiled the δ^{34}S of sedimentary pyrite, carbonate-associated sulfate, sulfate evaporites, and barite over Phanerozoic time. We interpolated

the values given in their Table A1 at intervals of 5 Myr to the times of interest (see Additional Data Table S1).

With the exception of a few densely sampled intervals, the seawater sulfate concentration data have sizable gaps (main text, Fig. 1A). Dramatic changes in sulfate concentration occur within intervals with no data (e.g. 350–300 Ma, 220–160 Ma). We specified changes in seawater sulfate concentration to be sigmoidal in shape and to pass through the clusters of more densely sampled periods. We note that future measurements of seawater sulfate concentrations during these barren intervals would improve our understanding of sulfur cycle processes.

SM Text

Neogene Evaporite Deposits and a Bias of Riverine Fluxes

We hypothesized that the modern riverine sulfate influx to the ocean may be anomalously high due to the deposition and subsequent exposure and weathering of Neogene-age evaporites. There is support for this notion from the macrostratigraphic obserations, as well as from previous studies. The estimated NAC per-area burial rate of sulfate evaporites in the bin centered 7.5 at Ma is anomalously high—2.8×10^4 mol yr^{-1} km^{-2} relative to an average of ~6.6×10^3 mol yr^{-1} km^{-2}, corrected for the effects of weathering (Fig. 1C of the main text). This value is exceeded only during ~4 intervals with anomalously high deposition rates. If the correction for decay of the record is not applied, the Messinian per-area rates of sulfate evaporite burial are approximately twice as high as the rates in any other Phanerozoic interval.

Evaporite deposits of Neogene age exist not only in North America and the Caribbean. Tectonics associated with the collision of Africa and Europe-Asia, as well as eustatic sea level changes, resulted in the formation and isolation of several marine-fed basins, causing several 'salinity crises'. Massive evaporite deposits formed in the Red Sea ~15 Ma (27), in the Carpathian foredeep during the Badenian salinity crisis, ~14 Ma (28), and all over the Mediterranean Sea during the Messinian salinity crisis, 5.96–5.33 Ma (29, 30). Many of these evaporites are exposed in Spain, France, Italy, Greece, Cyprus, Turkey, Lebanon, Egypt, Morocco, Poland and Ukraine, among other locations. These and other sulfates are exposed in a variety of locations today (e.g., 31), and contribute significantly to the riverine sulfate influx to the ocean.

We ask more generally whether the past ~10 Myr are special in having seen very high sulfate burial rates, or whether they simply record high rates by virtue of being young. The dependence of estimated deposition rates on the timescale of observation is well understood to represent the effect of depositional hiatuses and erosion on the long-term net rate (32). We hypothesize that the marked deviation of the recent apparent evaporite burial rate from the Phanerozoic average is the transient accumulation of stratigraphic deposits that will ultimately not be preserved. The fluxes associated with the deposition of these rocks and with their subsequent weathering will ultimately not affect seawater sulfate concentrations, if observed retrospectively. Inasmuch as the isotopic composition of these sulfate deposits is similar to the value of seawater sulfate during the past 10 Myr (which is itself approximately similar to the present-day ocean—~22‰ instead of ~21‰ VCDT; 46), their deposition and weathering will not strongly affect the long-term isotopic composition of seawater sulfate. The magnitude and isotopic

composition of riverine sulfate fluxes, however, will be strongly influenced by the weathering of these recent deposits, and consequently the instantaneous riverine fluxes may not be representative of the net supply or isotopic composition of sulfate to the oceans.

The contribution from recycling of recent evaporite deposits to the riverine flux can be broadly estimated. The total influx into the ocean, J_{in}, is:

$$(10) \qquad J_{in} = J_v + J_{pw} + J_{ew} + J_r,$$

where J_v is the volcanic influx, J_{pw} and J_{ew} are fluxes from oxidative weathering of pyrite and weathering of sulfate evaporites, respectively, and J_r is a flux from weathering of recently deposited evaporites. Assuming steady state, which the models broadly support, and approximating the fractional contribution to the influx from evaporite weathering and from oxidative weathering of pyrite to be similar to their fractional burial, J_{pw} and J_{ew} can be expressed as:

$$(11) \qquad J_{pw} = f_{pyr}(J_{in} - J_v - J_r),$$
$$(12) \qquad J_{ew} = (1 - f_{pyr})(J_{in} - J_v - J_r).$$

The isotopic composition of the total influx is:

$$(13) \qquad J_{in}\delta_{in} = J_v\delta_v + J_{pw}(\delta - \Delta) + J_{ew}\delta + J_r\delta.$$

Substituting (11) & (12) into (13) and rearranging for J_r yields:

$$(14) \qquad J_r = \frac{J_{in}\delta_{in} - J_v\delta_v - (J_{in} - J_v)f_{pyr}(\delta - \Delta) - (J_{in} - J_v)(1 - f_{pyr})\delta}{\delta - f_{pyr}(\delta - \Delta) - (1 - f_{pyr})\delta}$$

Substituting J_{in}=2.1, δ_{in}=8, J_v=0.3, δ_v=2, δ=21 and Δ=40‰ from the literature (8, 11, 12, 24, 44), and modern f_{pyr}=0.82 from this study (model of submerged continental area-dependent J_p), and solving yields J_r about 43–65% of the total influx.
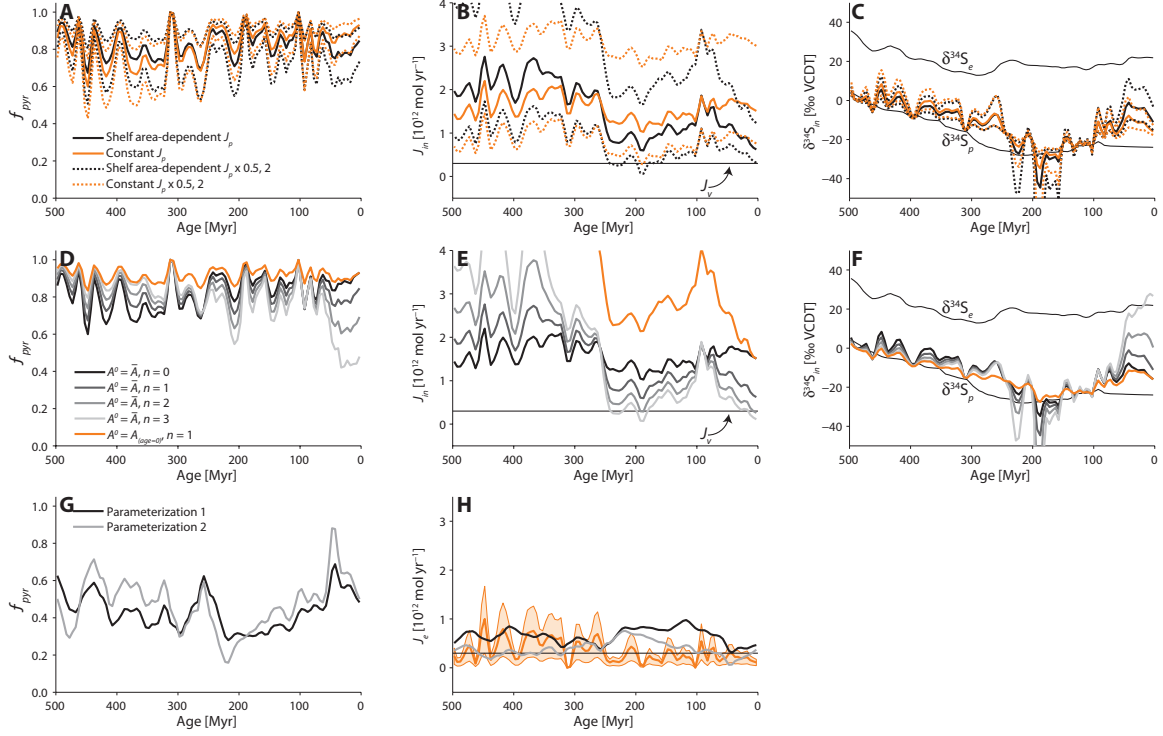
Fig. S1.

Sensitivity of model results to key parameters. (**A**) The effect on calculated f_{pyr} of doubling and halving the default value of J_p in the model of constant and submerged continental area-dependent J_p. All models still maintain a relatively high average value of f_{pyr} (0.6 or higher). (**B–C**) The effect of the same parameter variations as in A on the value of J_{in} and δ_{in}, respectively. (**D**) f_{pyr} calculated with a variable dependence of J_p on submerged continental area (n) and with different values of the reference submerged continental area (A^0). The average value of f_{pyr} remains high for all models. (**E–F**). J_{in} and δ_{in} calculated with the same parameter variation as in D. (**G**) The effect on calculated f_{pyr} of multiplying the assumed inputs from evaporite weathering and oxidative weathering of pyrite by 30% in the models of parameterized input fluxes. (**H**) The effect on the value of J_e^* (equation 8) required for mass balance in the parameterized input models. With influxes at 30% their full value, the magnitude of J_e^* is similar to the macrostratigraphic estimates of J_e.
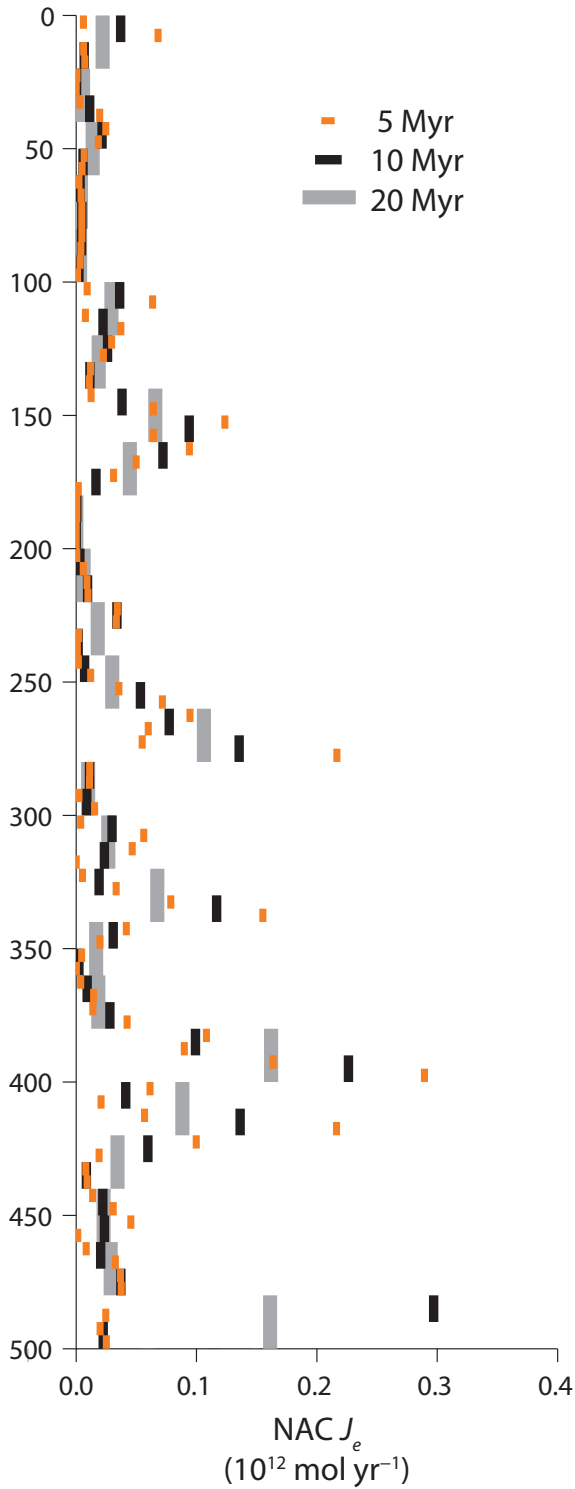
Fig. S2

Sulfate evaporite burial rates from North America and the Caribbean, binned into intervals of 5, 10 and 20 Myr. With increasing bin duration the variability in the record decreases, but mass is conserved by the binning process and the average remains unchanged.

Fig. S3
The geographic locations and areal extent of 949 stratigraphic columns in the Macrostrat database in North America, the Caribbean region and parts of Greenland, which were included in this study.
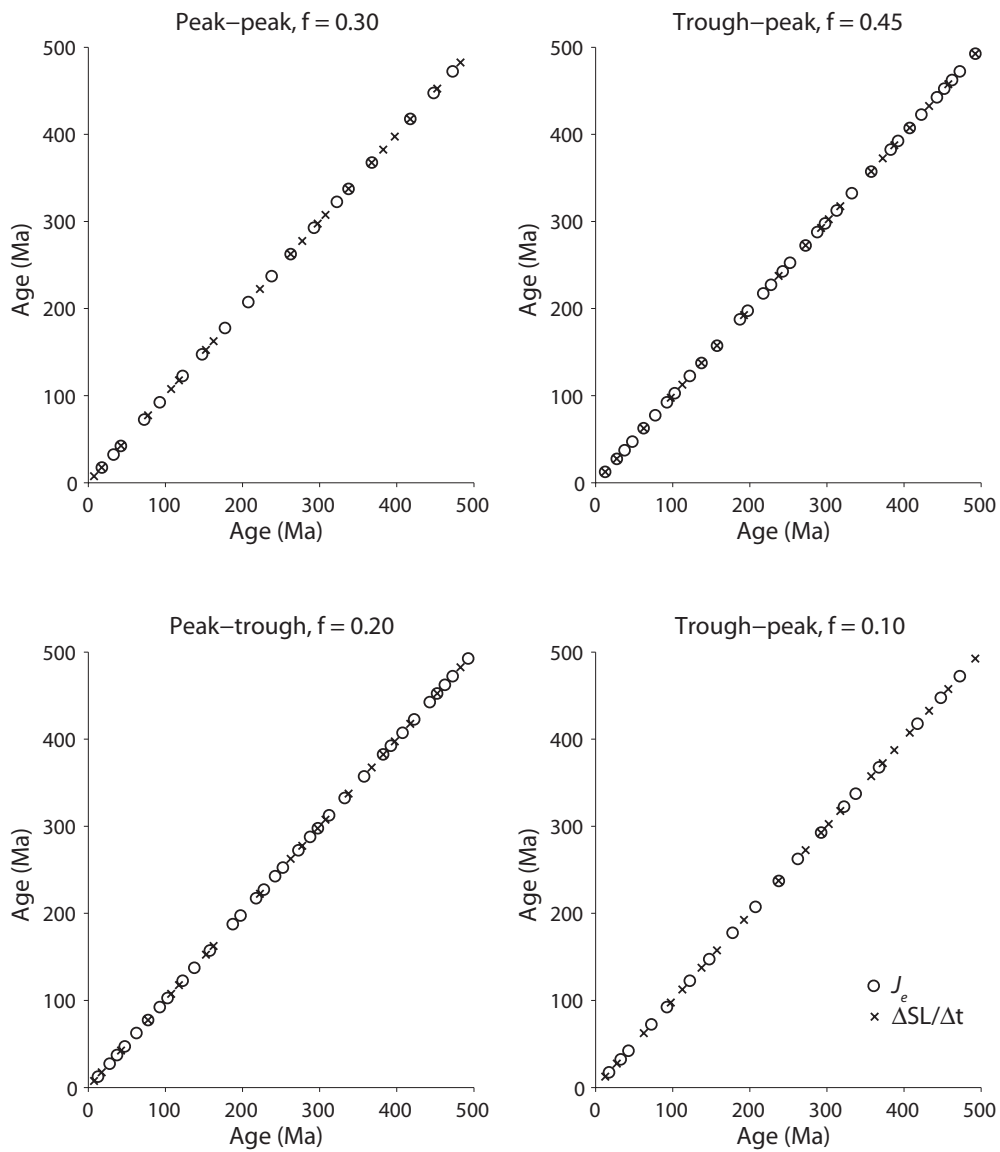
Fig. S4

Co-occurrence of peaks and troughs in sulfate burial rates and the rate of change of the global average sea level. About 30% of peaks in sulfate deposition and burial co-occur with maxima in sea level rise rates and about 45% of lows in sulfate deposition and burial co-occur with maxima in sea level fall rates.
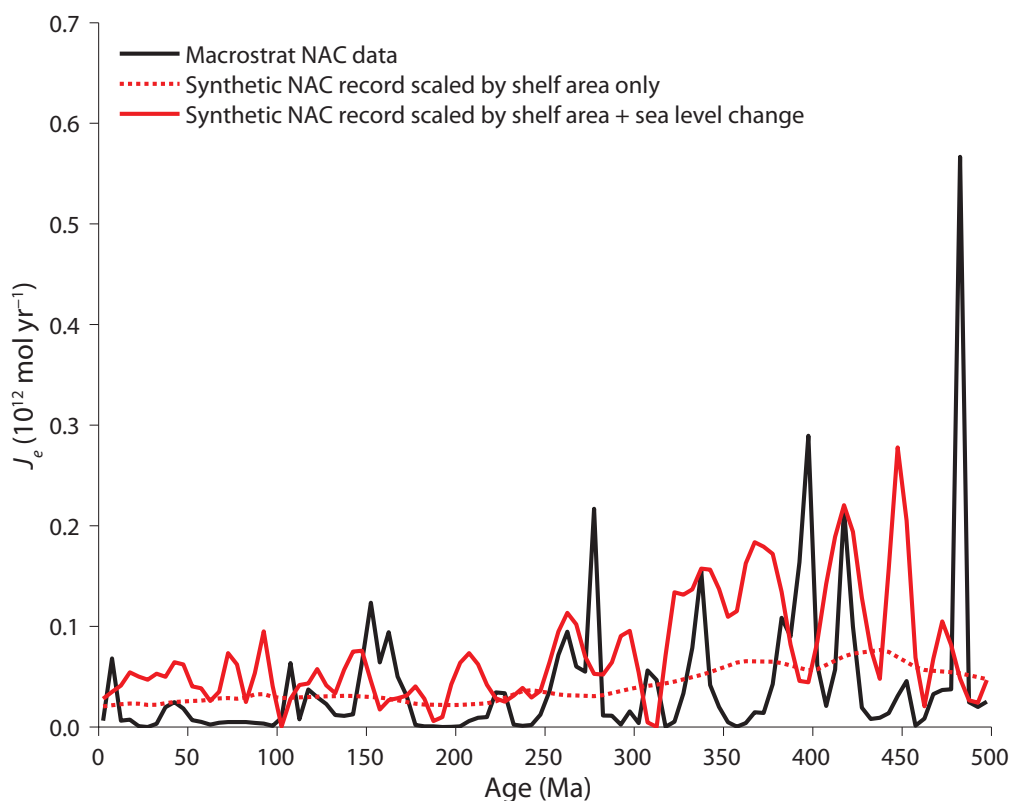
Fig. S5

A comparison of the sulfate burial record estimated from the macrostratigraphic data with a synthetic sulfate burial record for North America and the Caribbean. The correlation with submerged continental area captures the long-timescale variability in the burial record, whereas the relationship with sea level change adds short-timescale variability.

Additional Data Table S1 (separate comma-separated, plain text file)

Data and model fluxes binned in 5 Myr intervals. Columns from left to right are: Age of lower interval boundary (Ma), age of upper interval boundary (Ma), age in interval middle (Ma), NAC evaporite burial rates uncorrected for weathering (10^{12} mol yr^{-1}), NAC submerged continental area (km^3), global submerged continental area (km^3), global relative sea level (m), NAC evaporite burial rates corrected for weathering and scaled globally (10^{12} mol yr^{-1}), seawater sulfate concentration (mM), seawater sulfate δ^{34}S (‰ VCDT, from CAS, evaporites and barites), sedimentary pyrite δ^{34}S (‰ VCDT), input parameterization 1 J_v, J_{ew}, J_{pw} (10^{12} mol yr^{-1}), input parameterization 2 J_v, J_{ew}, J_{pw} (10^{12} mol yr^{-1}), δ_v (‰ VCDT), δ_{ew} (‰ VCDT), δ_{pw} (‰ VCDT).

References and Notes

1. F. M. M. Morel, J. G. Hering, *Principles and Applications of Aquatic Chemistry* (Wiley, New York, 1993).

2. B. B. Jørgensen, Mineralization of organic matter in the sea bed—the role of sulphate reduction. *Nature* **296**, 643 (1982). doi:10.1038/296643a0

3. R. A. Berner, Sedimentary pyrite formation: An update. *Geochim. Cosmochim. Acta* **48**, 605 (1984). doi:10.1016/0016-7037(84)90089-9

4. R. A. Berner, Models for carbon and sulfur cycles and atmospheric oxygen; application to Paleozoic geologic history. *Am. J. Sci.* **287**, 177 (1987). doi:10.2475/ajs.287.3.177

5. D. E. Canfield, The early history of atmospheric oxygen: Homage to Robert M. Garrels. *Annu. Rev. Earth Planet. Sci.* **33**, 1 (2005). doi:10.1146/annurev.earth.33.092203.122711

6. $\delta^{34}S = ({}^{34}R_{sam}/{}^{34}R_{ref} - 1) \times 1000$, where ${}^{34}R$ is the ratio of ${}^{34}S$ to ${}^{32}S$.

7. H. Strauss, The isotopic composition of sedimentary sulfur through time. *Palaeogeogr. Palaeocl.* **132**, 97 (1997). doi:10.1016/S0031-0182(97)00067-9

8. N. P. Wu, J. Farquhar, H. Strauss, S. T. Kim, D. E. Canfield, Evaluating the S-isotope fractionation associated with Phanerozoic pyrite burial. *Geochim. Cosmochim. Acta* **74**, 2053 (2010). doi:10.1016/j.gca.2009.12.012

9. T. K. Lowenstein, M. N. Timofeeff, S. T. Brennan, L. A. Hardie, R. V. Demicco, Oscillations in Phanerozoic seawater chemistry: evidence from fluid inclusions. *Science* **294**, 1086 (2001). doi:10.1126/science.1064280 Medline

10. J. Horita, H. Zimmermann, H. D. Holland, Chemical evolution of seawater during the Phanerozoic. *Geochim. Cosmochim. Acta* **66**, 3733 (2002). doi:10.1016/S0016-7037(01)00884-5

11. R. M. Garrels, A. Lerman, Coupling of the sedimentary sulfur and carbon cycles; an improved model. *Am. J. Sci.* **284**, 989 (1984). doi:10.2475/ajs.284.9.989

12. D. E. Canfield, The evolution of the Earth surface sulfur reservoir. *Am. J. Sci.* **304**, 839 (2004). doi:10.2475/ajs.304.10.839

13. A. Kampschulte, H. Strauss, The sulfur isotopic evolution of Phanerozoic seawater based on the analysis of structurally substituted sulfate in carbonates. *Chem. Geol.* **204**, 255 (2004). doi:10.1016/j.chemgeo.2003.11.013

14. D. B. Rowley, Rate of plate creation and destruction: 180 Ma to present. *Geol. Soc. Am. Bull.* **114**, 927 (2002). doi:10.1130/0016-7606(2002)114<0927:ROPCAD>2.0.CO;2

15. J. M. Edmond, Y. Huh, in *Tectonic Uplift and Climate Change*, W. F. Ruddiman, W. Prell, Eds. (Plenum, New York, 1997), pp. 329–351.

16. A. B. Ronov, The Earth's sedimentary shell (quantitative patterns of its structure, compositions, and evolution). *Int. Geol. Rev.* **24**, 1313 (1982). doi:10.1080/00206818209451075

17. M. A. Zharkov, *History of Paleozoic Salt Accumulation*, A. L. Yanshin, Ed. (Springer, New York, 1981).

18. R. A. Berner, A model for calcium, magnesium and sulfate in seawater over Phanerozoic time. *Am. J. Sci.* **304**, 438 (2004). doi:10.2475/ajs.304.5.438

19. S. E. Peters, N. A. Heim, The geological completeness of paleontological sampling in North America. *Paleobiology* **36**, 61 (2010). doi:10.1666/0094-8373-36.1.61

20. Methods are available on *Science* Online.

21. C. R. Scotese, *Atlas of Earth History* (PALEOMAP Project, Arlington, TX, 2001).

22. J. K. Warren, Evaporites through time: Tectonic, climatic and eustatic controls in marine and nonmarine deposits. *Earth Sci. Rev.* **98**, 217 (2010). doi:10.1016/j.earscirev.2009.11.004

23. B. U. Haq, A. M. Al-Qahtani, Phanerozoic cycles of sea-level change on the Arabian Platform. *GeoArabia* **10**, 127 (2005).

24. L. R. Kump, R. M. Garrels, Modeling atmospheric O_2 in the global sedimentary redox cycle. *Am. J. Sci.* **286**, 337 (1986). doi:10.2475/ajs.286.5.337

25. D. E. Canfield, R. Raiswell, The evolution of the sulfur cycle. *Am. J. Sci.* **299**, 697 (1999). doi:10.2475/ajs.299.7-9.697

26. R. Raiswell, Iron transport from the continents to the open ocean: The aging-rejuvenation cycle. *Elements* **7**, 101 (2011). doi:10.2113/gselements.7.2.101

27. J. M. Rouchy, D. Noel, A. M. A. Wali, M. A. M. Aref, Evaporitic and biosiliceous cyclic sedimentation in the Miocene of the Gulf of Suez—Depositional and diagenetic aspects. *Sediment. Geol.* **94**, 277 (1995). doi:10.1016/0037-0738(94)00095-C

28. T. M. Peryt, The beginning, development and termination of the Middle Miocene Badenian salinity crisis in Central Paratethys. *Sediment. Geol.* **188–189**, 379 (2006). doi:10.1016/j.sedgeo.2006.03.014

29. W. Krijgsman, F. J. Hilgen, I. Raffi, F. J. Sierro, D. S. Wilson, *Nature* **400**, 652 (1999). doi:10.1038/23231

30. J. M. Rouchy, A. Caruso, The Messinian salinity crisis in the Mediterranean basin: A reassessment of the data and an integrated scenario. *Sediment. Geol.* **188–189**, 35 (2006). doi:10.1016/j.sedgeo.2006.02.005

31. H. Rahimpour-Bonab, Z. Shariatinia, M. G. Siemann, Origin and geochemistry of Miocene marine evaporites associated with red beds: Great Kavir Basin, Central Iran. *Geol. J.* **42**, 37 (2007). doi:10.1002/gj.1069

32. P. M. Sadler, The influence of hiatuses on sediment accumulation rates. *GeoResearch Forum* **5**, 15 (1999).

33. S. E. Peters, Macrostratigraphy of North America. *J. Geol.* **114**, 391 (2006). [doi:10.1086/504176](#)

34. B. C. Gill *et al*., Geochemical evidence for widespread euxinia in the later Cambrian ocean. *Nature* **469**, 80 (2011). [doi:10.1038/nature09700](#) [Medline](#)

35. R. J. W. Douglas, *Geology and Economic Minerals of Canada*. Canada Geological Survey Economic Geology Report (1970).

36. O. E. Childs, Correlation of stratigraphic units of North America; COSUNA. *AAPG Bull.* **69**, 173 (1985).

37. A. Salvador, Chronostratigraphic and geochronometric scales in COSUNA stratigraphic correlation charts of the United States. *AAPG Bull.* **69**, 181 (1985).

38. C. N. Wold, W. W. Hay, Estimating ancient sediment fluxes. *Am. J. Sci.* **290**, 1069 (1990). [doi:10.2475/ajs.290.9.1069](#)

39. L. J. Walker, B. H. Wilkinson, L. C. Ivany, Continental drift and Phanerozoic carbonate accumulation in shallow-shelf and deep-marine settings. *J. Geol.* **110**, 75 (2002). [doi:10.1086/324318](#)

40. W. W. Hay *et al*., Evaporites and the salinity of the ocean during the Phanerozoic: Implications for climate, ocean circulation and life. *Palaeogeogr Palaeocl* **240**, 3 (2006). [doi:10.1016/j.palaeo.2006.03.044](#)

41. A. M. Ziegler *et al*., Tracing the tropics across land and sea: Permian to present. *Lethaia* **36**, 227 (2003). [doi:10.1080/00241160310004657](#)

42. C. Kerans, S. W. Tinker, in *Geologic framework of the Capitan Reef*, SEPM Special Publication 65 (Society for Sedimentary Geology, Tulsa, OK, 1999), pp. 15–36 (2000).

43. J. C. Alt, in *Seafloor Hydrothermal Systems, Physical, Chemical, Biological and Geological Interactions*, S. E. Humphries, R. A. Zierenberg, L. S. Mullineaux, R. E. Thomson, Eds. (American Geophysical Union, Washington, DC, 1995), pp. 85–114.

44. A. C. Kurtz, L. R. Kump, M. A. Arthur, J. C. Zachos, A. Paytan, Early Cenozoic decoupling of the global carbon and sulfur cycles. *Paleoceanography* **18**, 1090 (2003). [doi:10.1029/2003PA000908](#)

45. D. Calmels, J. Gaillardet, A. Brenot, C. France-Lanord, Sustained sulfide oxidation by physical erosion processes in the Mackenzie River basin: Climatic perspectives. *Geology* **35**, 1003 (2007). [doi:10.1130/G24132A.1](#)

46. A. Paytan, M. Kastner, D. Campbell, M. H. Thiemens, Sulfur isotopic composition of cenozoic seawater sulfate. *Science* **282**, 1459 (1998). [doi:10.1126/science.282.5393.1459](#) [Medline](#)